Journal of Hazardous Materials 171 (2009) 995–1000

Contents lists available at ScienceDirect

Journal of Hazardous Materials

journal homepage: www.elsevier.com/locate/jhazmat

Experimental assessment of adsorption of Cu^{2+} and Ni^{2+} from aqueous solution by oyster shell powder

Ting-Chu Hsu*

General Education Center, Nano Materials Applications R&D Center and Department of Environmental Engineering, Vanung University, Chung-Li 320, Taiwan

ARTICLE INFO

Article history:
Received 9 January 2009
Received in revised form 17 June 2009
Accepted 19 June 2009
Available online 26 June 2009

Keywords:
Oyster shell powder
Cu^{2+}
Ni^{2+}
Thermodynamics
Kinetics

ABSTRACT

In this study, I found that oyster shell powder (OSP) can effectively adsorb Cu^{2+} and Ni^{2+} from wastewater, with the adsorption capacity being higher for the former ion. The isotherms for the adsorption of Cu^{2+} and Ni^{2+} on the OSP fitted the Langmuir, Freundlich, and Dubinin–Kaganer–Radushkevich isotherms quite well (R^2 = 0.949–0.984, 0.912–0.988 and 0.900–0.990, respectively). Positive values of ΔH° and ΔS° indicated that these adsorptions were endothermic in nature; the values of E (between 1.722 and 3.553 kJ mol^{-1}) were consistent with a physical adsorption mechanism. Moreover, the adsorptions of Cu^{2+} and Ni^{2+} on the OSP followed pseudo-second-order kinetics. The adsorption capacities of the OSP toward Cu^{2+} and Ni^{2+} were 49.26–103.1 and 48.75–94.3 mg g^{-1}, respectively.

1. Introduction

Electroplating and metalworking industries discharge large amounts of heavy metals, including copper (Cu) and nickel (Ni) ions, in their effluents. Copper is highly toxic because it is non-biodegradable and carcinogenic [1–5]; the effects of Ni exposure vary from skin irritation to damage of the lungs, nervous system, and mucous membranes [6]. Several processing techniques are available to reduce the concentrations of heavy metals in wastewater, including precipitation, flotation, ion exchange, solvent extraction, adsorption, cementation onto iron, membrane processing, and electrolytic methods [2].

Adsorption onto activated carbon is a well-known method for removing toxic metal ions, but the high cost of activated carbon restricts its use in developing countries, with small factories in particular often being unable to support expensive wastewater treatment methods. Cheap and effective alternatives for the removal of heavy metals should reduce operating costs, reduce the prices of products, improve competitiveness, and benefit the environment. The adsorption abilities of a number of low-cost adsorbents (e.g., cheap zeolites, clay, coal fly ash, sewage sludge, agriculture waste and biomass) have been determined for the removal of heavy metals from water [7–13]. Another potential approach is the use of waste oyster shells: oysters abound on the west coast of Taiwan and waste oyster shell production exceeds 0.12 million tons per year. It is difficult to treat and dispose of such a huge amount of waste oyster shells. Furthermore, if the waste is left untreated for long time, it can be a source of noxious odors as a consequence of the decaying remnant flesh attached to the shells forming such gases as NH_3, H_2S, and amines. To solve these problems, I am seeking new applications for oyster shell powder (OSP) to increase the extent of oyster shell recycling.

In recent years, OSPs have been used as additives in construction materials and fish fodder, but their potential application as adsorbents are less well understood. I undertook this investigation to evaluate the effectiveness of employing an OSP for the adsorptive removal of Cu^{2+} and Ni^{2+} from wastewater, using experimental batch kinetic and isotherm studies to determine the adsorption capacities.

2. Materials and methods

2.1. Adsorbents

The raw OSP used in this study was purchased from the Long-Shin industrial company in Taiwan. It was dialyzed against distilled water (until pH < 10) to remove some excess alkalinity and chloride, then stored in a desiccator prior to use. This OSP after dialyzing comprised SiO_2 (30.7%), Al_2O_3 (6.8), $CaCO_3$ (60.5%), MgO (0.02%), Fe_2O_3 (1.83%), and SO_3 (0.05%). From the analysis of N_2 isotherms, the porous structure featured a BET surface area of 15.20 m^2 g^{-1}, an average pore size of 0.46 nm, and an average pore volume of 0.04 cm^3 g^{-1}.

* Tel.: +886 343 42379x46; fax: +886 346 22232.
E-mail address: djshue@mail.vnu.edu.tw.

0304-3894/$ – see front matter © 2009 Elsevier B.V. All rights reserved.
doi:10.1016/j.jhazmat.2009.06.105

2.2. Adsorbate

$Cu(NO_3)_2{\cdot}5H_2O$ and $Ni(NO_3)_2{\cdot}5H_2O$ were obtained in analytical grade (Merck Co.) and used without further purification.

2.3. Adsorption and kinetics studies

The Cu^{2+} and Ni^{2+} adsorption isotherms in aqueous solutions were obtained using the immersion method. Prior to use, the adsorbents were dried at 105 °C for 24 h to remove moisture. The adsorption of Cu^{2+} and Ni^{2+} was studied after adding 0.06 g of the adsorbent into an aqueous solution containing desired Cu^{2+} and Ni^{2+} concentrations (0–200 mg L^{-1}), adjusting the pH of the solution to 2, and shaking for 4 h at 30 °C. The equilibrium time was determined by studies of the adsorption kinetics. Because the adsorption equilibrium was established within 3–4 h, the contact time was fixed at 4 h. For thermodynamic studies, these procedures were repeated at 45 and 60 °C. Because the values of pH of the effluents from electroplating and metalworking industries are close to 2, for direct applicability to treating real wastewater samples, the pH of the solution was fixed at 2 in this study. I also studied the blank tests and found no significant ions released from the OSP at the adsorption conditions.

2.4. Equipment

The surface area and total pore volume of the OSP were measured through N_2 adsorption at temperatures below 77 K using a Micromeritics TRISTAR-3000 apparatus. The OSP was outgassed with He at 105 °C for 16 h prior to performing the adsorption measurement. The resulting suspensions were filtered and the solution was analyzed using a Hitachi 1100B atomic absorption spectrophotometer (AAS). The pH of each solution was determined using a JenCo 1671 pH meter. The mineral surface and sorbed pollutants on the surface were analyzed using a PerkinElemer Model 1600 Fourier transform infrared (FTIR) spectrometer.

2.5. Errors

The maximum error observed in liquid-phase concentration measurements was 0.5 mg L^{-1}. The triplicates of isotherm and kinetics measurements were achieved to within ±5% of the measured values presented here.

3. Results and discussion

3.1. Effect of temperature

Fig. 1 reveals that the maximum adsorption capacity occurred at 60 °C for each of the two adsorbates; their adsorption capacities followed the order 60 °C > 45 °C > 30 °C. This increase in adsorption upon increasing the temperature indicates an endothermic nature for each of these adsorption processes.

3.2. Amounts of Cu^{2+} and Ni^{2+} adsorbed on the OSP

Fig. 1 indicates that the amount of Cu^{2+} adsorbed on the OSP was larger than that of Ni^{2+} at each of three different temperatures (30, 45, and 60 °C). It is clear that the OSP sample exhibited superior performance toward the adsorption of Cu^{2+}.

3.3. Effect of contact time

Fig. 2 displays the effects of the contact time on the amount of Cu^{2+} and Ni^{2+} adsorbed per unit of adsorbent at three different temperatures (30, 45, and 60 °C). For Cu^{2+} and Ni^{2+}, a gradual increase in adsorption occurred upon increasing the contact time up to 120–240 min, at which point the maximum values of adsorption were attained. Extending the contact time further had an insignificant effect on the amounts of the heavy metals adsorbed. For this reason, I used a contact time of 240 min as the optimum value in our subsequent experiments.

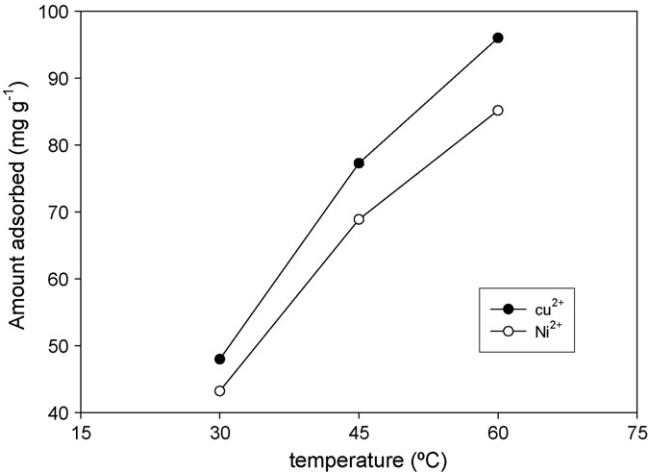

Fig. 1. Adsorption capacities of OSP toward Cu^{2+} and Ni^{2+} at various temperatures.

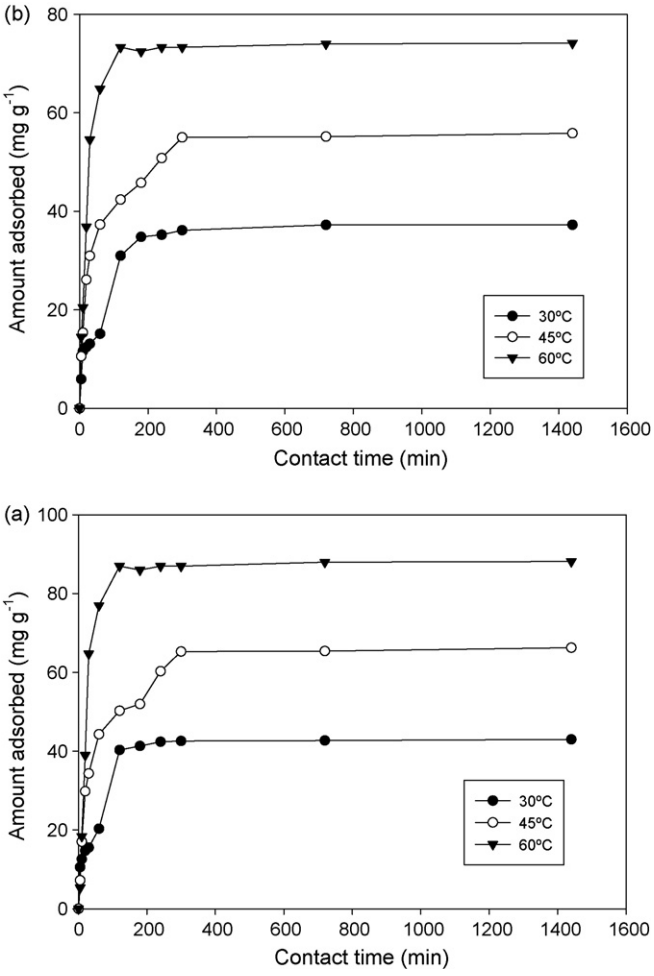

Fig. 2. Contact times for the adsorptions of (a) Cu^{2+} and (b) Ni^{2+} onto OSP at various temperatures.

Table 1
Adsorption capacities of Cu^{2+} and Ni^{2+} on various low-cost adsorbents.

Adsorbent	Cu^{2+} (mg g^{-1})	Ni^{2+} (mg g^{-1})	Reference
Chabazite	5.10	4.50	[10]
Jordanian zeolites	25.00–47.50	23.70–52.5	[10]
Coal fly ash	178.5–249.1		[17]
Bagasse fly ash	2.26–2.36		[17]
Fly ash + wollastonite	1.18		[10]
Peat moss	6.41–19.56	11.15–11.74	[10]
Industrial waste	13.80–23.66	160.0	[8,10]
Sewage sludge	3.282–30.70		[7,9]
Citrus reticulata		158.0	[10]
Brown algae	47.63–102.9	48.72–58.11	[11]
Chitosan	7.40–222.0	2.40	[10]
Oyster shell powder	49.26–103.1	48.75–94.30	This study

3.4. Adsorption isotherms

Table 1 compares the adsorption capacities of various low-cost adsorbents for Cu^{2+} and Ni^{2+}, determined by us and others; the adsorption capacities of Cu^{2+} and Ni^{2+} were in the ranges 1.18–249.1 and 2.40–160.0 mg g^{-1}, respectively. In addition, I used the well-known Langmuir and Freundlich models to analyze the results obtained for the adsorptions of Cu^{2+} and Ni^{2+} onto the OSP samples. The Langmuir isotherm assumes a completely homogeneous surface, whereas the Freundlich isotherm is suitable for highly heterogeneous surfaces. In addition to the Langmuir and Freundlich isotherms, I also examined the Dubinin–Kaganer–Radushkevich (DKR) isotherm.

3.4.1. Langmuir isotherm

The Langmuir isotherm is the most commonly used isotherm for analyzing the sorptions of various compounds. In its linear form, it can be represented as follows:

$$\frac{1}{Q_e} = \frac{1}{Q_0} + \frac{1}{bQ_0C_e} \quad (1)$$

where Q_e is the amount adsorbed (mg g^{-1}), C_e is the equilibrium concentration of the adsorbate (mg L^{-1}), and Q_0 and b are Langmuir constants related to the maximum adsorption capacity and energy of adsorption, respectively. When $1/Q_e$ is plotted against $1/C_e$, a straight line having a slope of $1/bQ_0$ and an intercept at $1/Q_0$ is obtained. I calculated the Langmuir constants Q_0 and b from Fig. 3. Table 2 provides these values for the adsorptions of Cu^{2+} and Ni^{2+} on the OSP samples. The values of R^2 are in the range of 0.949–0.984, revealing that these adsorption events fit the Langmuir isotherm quite well. For both adsorbates, the maximum adsorption capacities (Q_0) followed the order 60 °C > 45 °C > 30 °C.

3.4.2. Freundlich isotherm

The Freundlich isotherm is most frequently used to describe the adsorption of inorganic and organic compounds in solution. In its logarithmic form, it can be represented as follows:

$$\log Q_e = \log K_F + \frac{1}{n}\log C_e \quad (2)$$

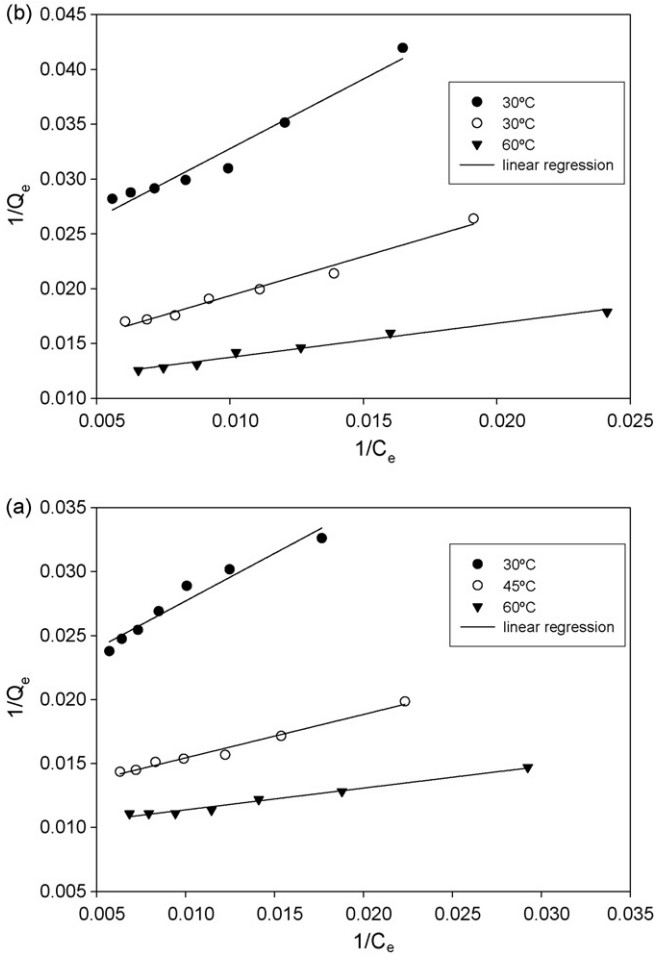

Fig. 3. Langmuir isotherms for the adsorptions of (a) Cu^{2+} and (b) Ni^{2+} onto OSP at various temperatures.

where Q_e is the amount adsorbed (mg g^{-1}), C_e is the equilibrium concentration of the adsorbate (mg L^{-1}), and K_F and n are Freundlich constants related to the adsorption capacity and adsorption intensity, respectively. When $\log Q_e$ is plotted against $\log C_e$, a straight line having a slope of $1/n$ and an intercept at $\log K_F$ is obtained. I used Fig. 4 to calculate the Freundlich constants K_F and n; Table 2 lists their values for the adsorptions of Cu^{2+} and Ni^{2+} on the OSP. Because the values of R^2 all fall in the range of 0.912–0.988, these adsorption events appear to follow the Freundlich isotherm quite well. In each case, the value of n was greater than 1, revealing that adsorption was a favorable process.

3.4.3. DKR isotherm

The DKR equation has been used previously to examine the mechanisms of the adsorptions of Cu^{2+} and Ni^{2+} onto various adsor-

Table 2
Langmuir and Freundlich constants for the adsorption of Cu^{2+} and Ni^{2+} onto OSP.

Adsorbate	Temperature (°C)	Langmuir			Freundlich		
		Q_0 (mg g^{-1})	b (L mg^{-1})	R^2	n	K_F	R^2
Cu^{2+}	30	49.26	0.027	0.949	3.475	9.456	0.986
	45	83.33	0.035	0.982	4.047	20.469	0.934
	60	103.1	0.057	0.984	4.998	34.66	0.925
Ni^{2+}	30	48.75	0.016	0.959	2.719	5.512	0.912
	45	81.97	0.017	0.980	2.662	9.003	0.950
	60	94.34	0.034	0.978	3.560	19.72	0.988

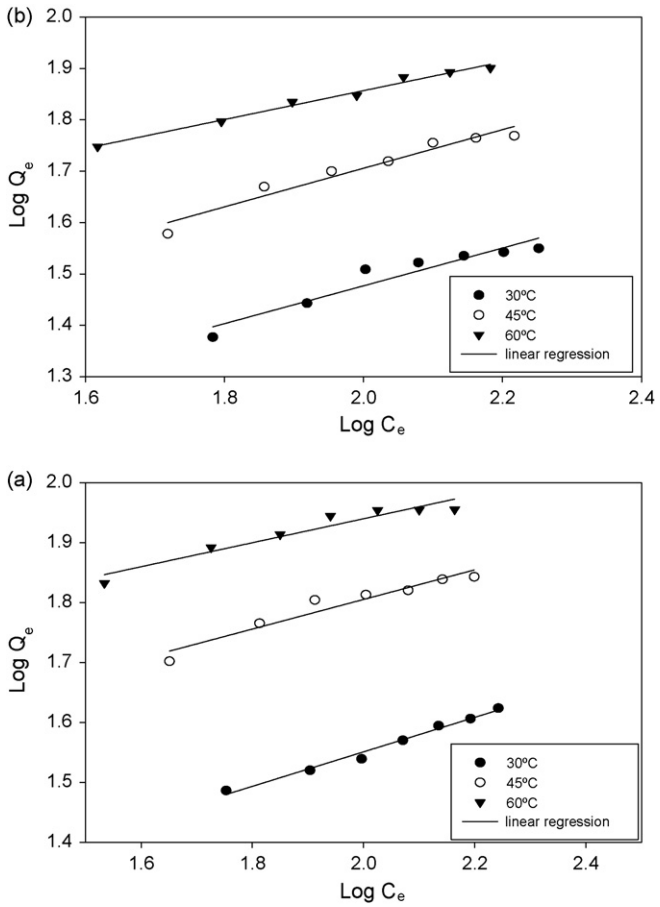

Fig. 4. Freundlich isotherms for the adsorptions of (a) Cu^{2+} and (b) Ni^{2+} onto OSP at various temperatures.

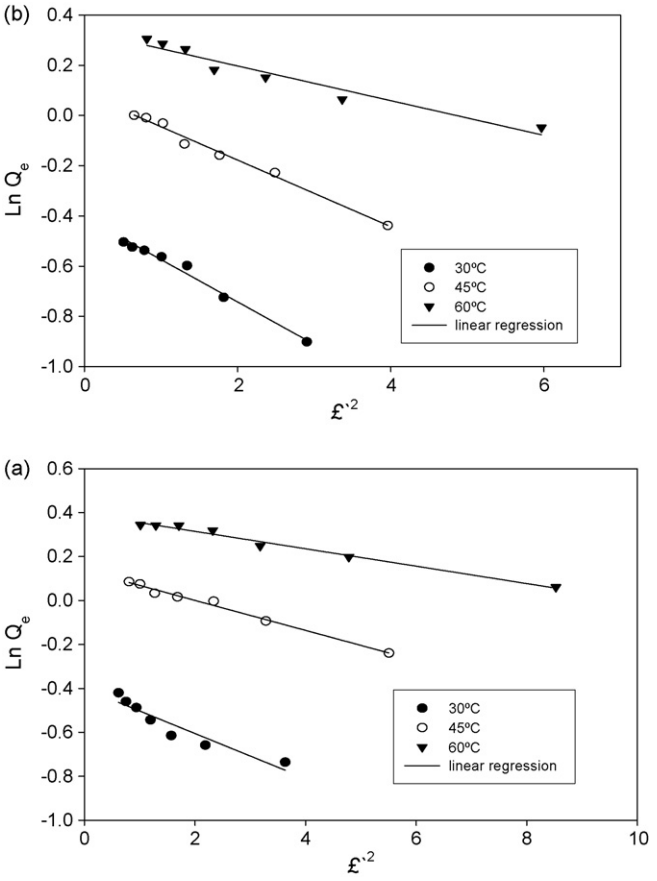

Fig. 5. DKR isotherms for the adsorptions of (a) Cu^{2+} and (b) Ni^{2+} onto OSP at various temperatures.

bents [14,15]. The DKR equation can be represented as follows:

$$\ln Q_e = \ln Q_m - \beta\varepsilon^2 \quad (3)$$

where Q_e is the amount adsorbed (mmol kg^{-1}), Q_m (mmol kg^{-1}) is the DKR monolayer capacity, β (mol^2 J^{-2}) is a constant related to the sorption energy, and ε is the Polanyi potential, which is related to the equilibrium concentration through the expression

$$\varepsilon = RT \ln\left(\frac{1}{C}\right), \quad (4)$$

where T is the temperature and C is the equilibrium concentration of Cu^{2+} or Ni^{2+} in solution. When $\ln Q_e$ is plotted against ε^2, a straight line is obtained having a slope of β and an intercept at Q_m. I calculated these values from the data in Fig. 5. The value of β is related to the sorption energy, E, through the following relationship:

$$E = \frac{1}{(-2\beta)^{1/2}} \quad (5)$$

Table 3 provides the DKR parameters and values of E for the sorptions of Cu^{2+} and Ni^{2+} on the OSP at various temperatures. Because the values of R^2 were in the range of 0.900–0.990, the adsorptions of Cu^{2+} and Ni^{2+} on the OSP appear to follow the DKR isotherm quite well.

The sorption process is dominated by particle diffusion. Indeed, our calculated adsorption energies for Cu^{2+} and Ni^{2+} (2.210–3.553 and 1.722–2.692 kJ mol^{-1}, respectively) suggest that the sorption processes are governed by physical adsorption mechanisms ($E < 8$ kJ mol^{-1}) at all temperatures [7,16].

3.5. Thermodynamic studies

Table 4 lists the thermodynamic parameters calculated using the following equations [17–19]:

$$\Delta G^\circ = -RT \ln b' \quad (6)$$

$$\ln\frac{b_2}{b_1} = -\left(\frac{\Delta H^\circ}{R}\right)\left[\frac{T_1 - T_2}{T_2 T_1}\right] \quad (7)$$

Table 3
DKR parameters for the adsorption of Cu^{2+} and Ni^{2+} onto OSP.

Adsorbate	Temperature (°C)	Q_m (mg g^{-1})	β (mol^2 J^{-2})	Sorption energy, E (kJ mol^{-1})	R^2
Cu^{2+}	30	42.89	-1.02×10^{-7}	2.210	0.900
	45	73.37	-6.82×10^{-8}	2.708	0.990
	60	87.01	-3.96×10^{-8}	3.553	0.984
Ni^{2+}	30	39.14	-1.69×10^{-7}	1.722	0.986
	45	64.08	-1.33×10^{-7}	1.942	0.990
	60	82.05	-6.90×10^{-8}	2.692	0.944

Table 4
Thermodynamic parameters for the adsorption of Cu^{2+} and Ni^{2+} onto OSP.

Adsorbate	ΔG° (kJ mol^{-1})			ΔH° (kJ mol^{-1})	ΔS° (J mol^{-1} K^{-1})
	30 °C	45 °C	60 °C		
Cu^{2+}	−18.81	−20.42	−22.41	20.88	130.2
Ni^{2+}	−20.0	−22.9	−26.4	44.90	127.7

$$\Delta S^\circ = \frac{\Delta H^\circ - \Delta G^\circ}{T} \quad (8)$$

where b', b_2, and b_1 are the Langmuir constants at T, T_2, and T_1, respectively. The negative values of ΔG° at all temperatures (Table 4) indicate that the adsorption processes are favorable and spontaneous. Moreover, the free energy decreased upon increasing the temperature; i.e., the adsorption events are favored at high temperatures. The positive values of ΔH° and ΔS° for each sample indicate that the processes are endothermic and aided by increased disorder. The increase in adsorption at higher temperatures also indicates the endothermic nature of these adsorption processes.

3.6. Kinetics adsorption studies

I analyzed the adsorption kinetics using several models, including the pseudo-first-order Lagergren equation [18,20] and a pseudo-second-order rate equation [21,22], represented by Eqs. (9) and (10), respectively, to examine the kinetics of the adsorption processes.

$$\ln(Q_e - Q_t) = \ln Q_e - k_1 t \quad (9)$$

$$\frac{t}{Q_t} = \left[\frac{1}{k_2 {Q_e}^2}\right] + \left(\frac{1}{Q_e}\right) t \quad (10)$$

where Q_t is the amount (mg g^{-1}) of material adsorbed at time t, Q_e is the adsorption capacity (mg g^{-1}) at equilibrium, k_1 is the rate constant (min^{-1}) of the pseudo-first-order model, and k_2 is the rate constant (g mg^{-1} min^{-1}) of the pseudo-second-order model. From the slopes and intercepts of these curves, I determined the values of k_1 and k_2 and the equilibrium capacity (Q_e). Figs. 6 and 7 present the experimental data for the different adsorbates fitted using the pseudo-first-order and pseudo-second-order kinetic models, respectively; Table 5 lists the resulting parameters obtained using both models. The pseudo-first-order model (R^2 = 0.703–0.992) did not represent the kinetics as well as those obtained using the pseudo-second-order kinetics model, where the high linearity of the plots of t/Q_t versus t (R^2 > 0.966) confirmed the pseudo-second-order nature of the process.

In the pseudo-second-order model, the product $k_2 {Q_e}^2$ is the initial sorption rate, h. Table 5 indicates that the pseudo-second-order rate constant (k_2) for Cu^{2+} reached its maximum value at 30 °C; it was maximized at 60 °C for Ni^{2+}. The maximum initial sorption rates (h) for Cu^{2+} and Ni^{2+} were 3.896 mg g^{-1} min^{-1} (60 °C) and 6.219 mg g^{-1} min^{-1} (60 °C), respectively. For the adsorption of Cu^{2+}

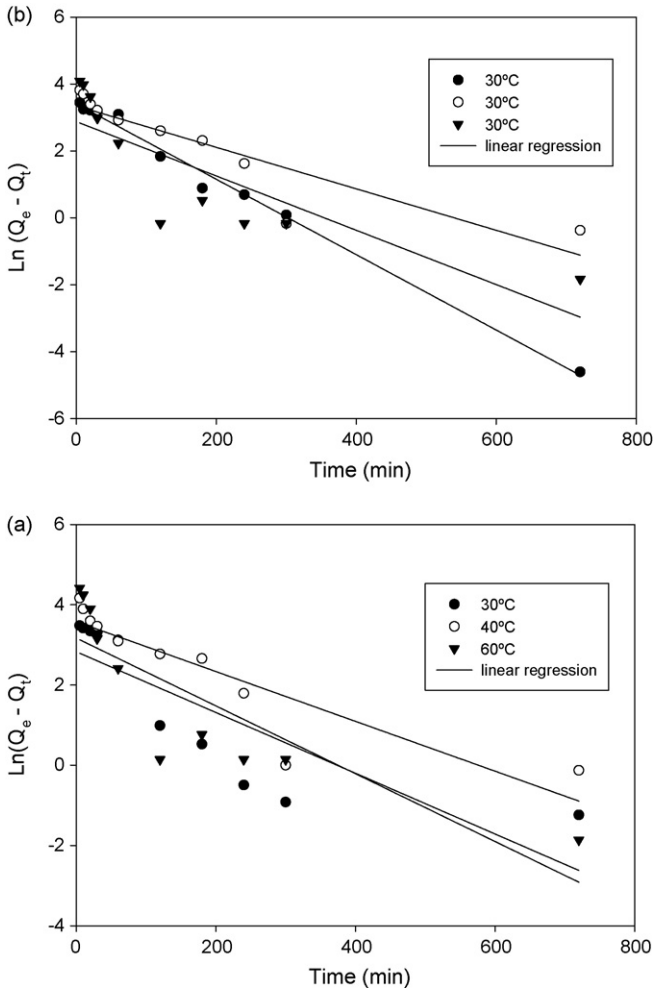

Fig. 6. Plots of the pseudo-first-order Lagergren equation for the adsorptions of (a) Cu^{2+} and (b) Ni^{2+} onto OSP at various temperatures.

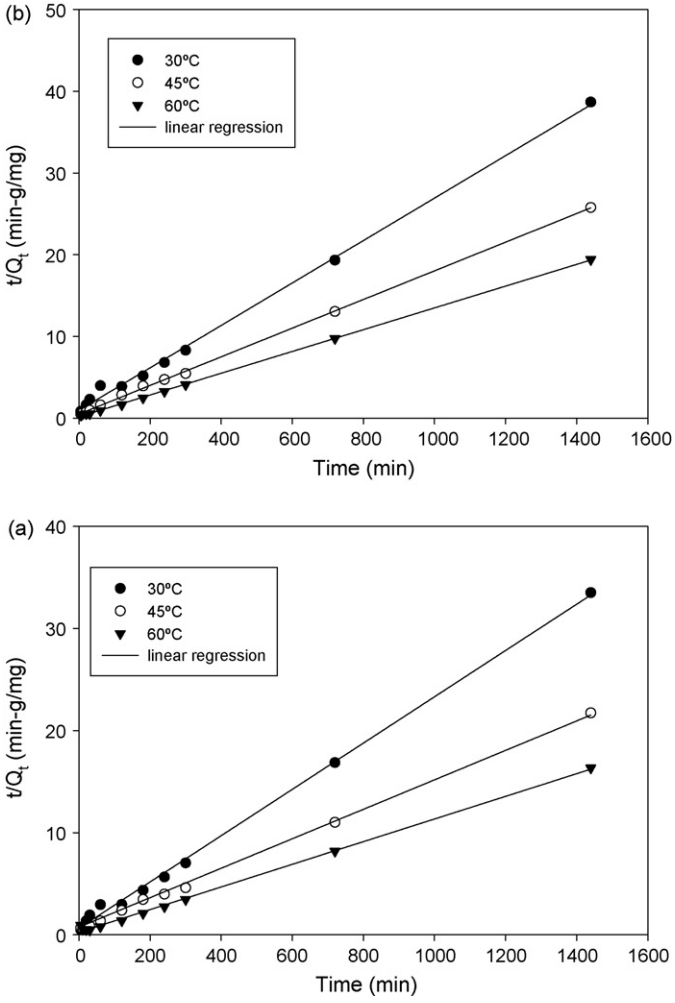

Fig. 7. Plots of the pseudo-second-order kinetics for the adsorptions of (a) Cu^{2+} and (b) Ni^{2+} onto OSP at various temperatures.

Table 5
Kinetic parameters for the adsorption of Cu^{2+} and Ni^{2+} onto OSP.

Adsorbate	Temperature (°C)	Pseudo-first-order		Pseudo-second-order			
		K_1 (min^{-1})	R^2	Q_e ($mg\,g^{-1}$)	K_2 ($g\,mg^{-1}\,min^{-1}$)	h ($mg\,g^{-1}\,min^{-1}$)	R^2
Cu^{2+}	30	7.6×10^{-3}	0.703	44.05	8.0×10^{-4}	1.552	0.998
	45	6.2×10^{-3}	0.798	68.03	4.4×10^{-4}	2.036	0.999
	60	8.5×10^{-3}	0.736	90.09	4.8×10^{-4}	3.895	0.998
Ni^{2+}	30	1.1×10^{-2}	0.992	38.46	7.0×10^{-4}	1.035	0.966
	45	6.2×10^{-3}	0.814	57.14	6.2×10^{-4}	2.024	0.999
	60	8.1×10^{-3}	0.706	75.19	1.1×10^{-3}	6.219	0.999

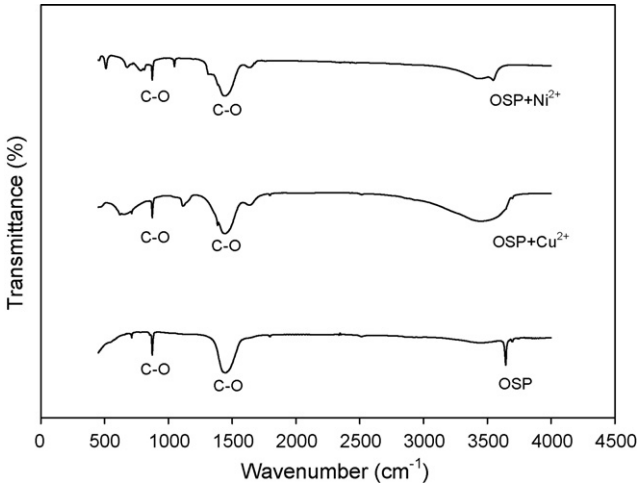

Fig. 8. FTIR spectra of the OSP in KBr disk, before and after adsorption of Cu^{2+} and Ni^{2+}.

and Ni^{2+} on the OSP, the sorption rates (h) all followed the order 60 °C > 45 °C > 30 °C.

3.7. FTIR spectroscopic analysis

To determine the functional groups responsible for metal uptake, I performed a solid phase FTIR spectroscopic analysis of the OSP prepared in a KBr disk. FTIR spectra were obtained for adsorbent solid samples before and after their adsorption events. The spectra in Fig. 8 display a number of adsorption peaks, indicating the nature of the material examined. The intensities of the C–O bands of $CaCO_3$ (OSP) between 1500 and 500 cm^{-1} were the strongest [23]. I observed C–O stretching vibration at 1440–1450 cm^{-1} and the out-of-plane C–O bending vibrations at 870–880 cm^{-1}. For the samples after adsorption, all of these peaks had substantially lower absorbances than those in the raw sample; the small differences in the frequencies of these bands suggest the physical adsorption of Cu^{2+} and Ni^{2+} by the OSP waste.

4. Conclusions

OSP is a cheap and effective adsorbent for the removal of Cu^{2+} and Ni^{2+} ions from wastewater without requiring any pretreatment. The adsorptions of Cu^{2+} and Ni^{2+} onto OSP are consistent with the Langmuir, Freundlich, and DKR isotherms. According to the calculated sorption energies ($E < 8\,kJ\,mol^{-1}$) and FTIR spectroscopic analysis, the adsorption processes occur through physical adsorption mechanisms. Kinetic and thermodynamic studies revealed that the adsorption processes were all endothermic and followed pseudo-second-order kinetics ($R^2 > 0.966$). According to the Langmuir isotherm, the adsorption capacities of OSP toward Cu^{2+} and Ni^{2+} were 49.26–103.1 and 48.75–94.34 $mg\,g^{-1}$, respectively.

Acknowledgment

I thank Vanung University for financial support.

References

[1] V. Boonamnuayvitaya, C. Chaiya, W. Tanthapanichakoon, S. Jarudilokkul, Removal of heavy metals by adsorbent prepared from pyrolyzed coffee residues and clay, Sep. Purif. Technol. 35 (2004) 11–22.
[2] F.A. Lopez, M.I. Martin, C. Perez, A. Lopez-Delgado, F.J. Alguacil, Removal of copper ion from aqueous solution by a steel-making by-product, Water Res. 37 (2003) 3883–3890.
[3] B.S. Krishna, N. Mahadevaiah, D.S.R. Murty, B.S. Jai Prakash, Surfactant immobilized interlay species bonded montmorillonite as recyclable adsorbent for lead ion, J. Colloid Interface Sci. 271 (2004) 270–276.
[4] V.K. Gupta, I. Ali, Utilisation of bagasse fly ash (a sugar industry waste) for the removal of copper and zinc from wastewater, Sep. Purif. Technol. 18 (2000) 131–140.
[5] K.S. Hui, C.Y.H. Chao, S.C. Kot, Removal of mixed heavy metal ions in wastewater by zeolite 4A and residual products from recycled coal fly ash, J. Hazard. Mater. 127 (2005) 89–101.
[6] M.E. Argun, S. Dursun, C. Ozdemir, M. Karatas, Heavy metal adsorption by modified oak sawdust: thermodynamics and kinetics, J. Hazard. Mater. 141 (2007) 77–85.
[7] S.C. Pan, C.C. Lin, D.H. Tseng, Reusing sewage sludge ash as adsorbent for copper removal from wastewater, Resour. Conserv. Recy. 39 (2003) 79–90.
[8] A. Lopez-Delogado, C. Perez, F.A. Lopez, Sorption of heavy metals on blast furnace sludge, Water Res. 32 (1998) 989–996.
[9] M. Oteroa, F. Rozada, A. Morán, L.F. Calvo, A.I. García, Removal of heavy metals from aqueous solution by sewage sludge based sorbents: competitive effects, Desalination 239 (2009) 46–57.
[10] S. Babel, T.A. Kurniawan, Low-cost adsorbents for heavy metals uptake from contaminated water: a review, J. Hazard. Mater. 97 (2003) 219–243.
[11] Y. Liu, Q. Cao, F. Luo, J. Chen, Biosorption of Cd^{2+}, Cu^{2+}, Ni^{2+} and Zn^{2+} ions from aqueous solutions by pretreated biomass of brown algae, J. Hazard. Mater. 163 (2009) 931–938.
[12] H. Cho, D. Oh, K. Kim, A study on removal characteristics of heavy metals from aqueous solution by fly ash, J. Hazard. Mater. 127 (2005) 187–195.
[13] F.S. Zhang, J.O. Nriagu, H. Itoh, Mercury removal from water using activated carbons derived from organic sewage sludge, Water Res. 39 (2005) 389–395.
[14] S.B. Wang, M. Soudi, L. Li, Z.H. Zhu, Coal ash conversion into effective adsorbents for removal of heavy metal and dyes from wastewater, J. Hazard. Mater. 133 (2006) 243–251.
[15] S.H. Lin, R.S. Juang, Heavy metal removal from water by sorption using surfactant-modified montmorillonite, J. Hazard. Mater. 92 (2002) 315–326.
[16] F. Helfferich, Ion Exchange, McGraw-Hill, New York, 1962.
[17] T.C. Hsu, C.C. Yu, C.M. Yeh, Adsorption of Cu^{2+} from water using raw and modified coal fly, Fuel 87 (2008) 1355–1359.
[18] T.C. Hsu, Adsorption of an acid dye onto coal fly ash, Fuel 87 (2008) 30740–30745.
[19] V.K. Gupta, I. Ali, Removal of lead and chromium from wastewater using bagasse fly ash-a sugar industry waste, J. Colloid Interface Sci. 271 (2004) 321–328.
[20] S. Lagergren, Zur theorie der sogenannten adsorption geloster stoffe. Kungliga Svenska Vetenkapsakademiens, Handlingar 24 (1898) 1–39.
[21] C.C. Wang, L.C. Juang, C.K. Lee, T.C. Hsu, J.F. Lee, H.P. Chao, Effect of exchanged surfactant cations on the pore structure and adsorption characteristics of montmorillonite, J. Colloid Interface Sci. 280 (2004) 27–35.
[22] C.C. Wang, L.C. Juang, T.C. Hsu, C.K. Lee, J.F. Lee, F.C. Huang, Adsorption of basic dyes onto montmorillonite, J. Colloid Interface Sci. 273 (2004) 80–86.
[23] W. Tongamp, J. Kano, Q. Zhang, F. Saito, Simultaneous treatment of PVC and oyster-shell wastes by mechanochemical means, Waste Manage. 28 (2008) 484–488.